JOM, Vol. 71, No. 4, 2019
https://doi.org/10.1007/s11837-019-03386-y

Interplay Between Grain Boundaries and Radiation Damage

CHRISTOPHER M. BARR,[1] OSMAN EL-ATWANI,[2] DJAMEL KAOUMI,[3] and KHALID HATTAR[1,4]

1.—Sandia National Laboratories, Albuquerque, NM 87185, USA. 2.—Los Alamos National Laboratory, Los Alamos, NM 87545, USA. 3.—North Carolina State University, Raleigh, NC 27607, USA. 4.—e-mail: khattar@sandia.gov

The need for enhanced radiation-tolerant materials for advanced nuclear energy designs has resulted in a growing number of investigations that have explored the effect of grain boundaries under irradiation. The key motivation for examining the role of grain boundaries in radiation environments is the ability to tailor grain boundary networks through either the introduction of specific grain boundaries or an increase in the grain boundary density. While traditionally thought to be efficient sinks for radiation-induced point defects, many recent experimental studies in model and pure systems have shown significant heterogeneity in grain boundary-defect interactions and associated sink efficiency as a function of grain boundary character. Furthermore, grain boundaries can migrate under irradiation, which creates an additional level of complexity. This article will provide a prospective on the experimental observations associated with defect evolution near grain boundaries including variation in sink efficiency and grain boundary mobility in radiation environments.

INTRODUCTION

Both current and next-generation nuclear energy systems require microstructures capable of providing structural integrity, while withstanding demanding irradiation conditions, high temperature, and environmental interactions.[1] Designing optimal microstructures for these demanding conditions requires careful consideration of the complex and fundamental interactions of grain boundaries (GBs) with irradiation damage. GB properties including mobility, energy, stiffness, and free volume have been shown to be highly anisotropic as a function of the structure.[2–7] Though complex, the heterogeneous nature of the local GB structure and overall GB network provide a design route to tailor the microstructural response under irradiation.

One route to improve materials response under irradiation and other demanding environments is GB sensitive design. GB sensitive design is broadly defined as any route to engineer or tailor either individual GBs or their network to improve a property or environmental response. With the concept of GB sensitive design central to this review article, we will assess the complex interplay between GBs and radiation damage. Previous review articles have shown the importance of similar interactions from both fundamental science and nuclear energy application perspectives[8,9] and have already explored various nanostructured systems in radiation environments including general nanostructured materials,[10,11] oxide dispersion-strengthened alloys,[8] nanostructured ferritic alloys,[12] and nanoscale multilayers,[13] and their associated mechanisms such as radiation-induced solute segregation (RIS)[14] as well as the design and processing concepts for radiation-tolerant materials.[13] Here, we will highlight two key insights, gained primarily through experimental investigations, that have contributed significantly to the current understanding of the fundamental interaction between radiation-induced damage and GBs in model and single-element metallic systems:

I. The role local GB structure plays in irradiation-induced defect spatial distribution and defect accommodation.
II. The role GB migration can play in the resultant microstructure and radiation response.

(Published online March 5, 2019)

DEFECT-GRAIN BOUNDARY INTERACTIONS

Heterogeneous Defect Evolution Near Grain Boundaries

It has been well established that GBs act as sinks for point defects and point defect clusters under irradiation.[15] The ability of GBs to annihilate and absorb point defects and defect clusters under irradiation provides a mechanism to locally reduce radiation damage. Research efforts over the past several decades[16–18] have therefore utilized the ability of GBs to mitigate radiation damage by optimizing the GB character distribution and GB density. Extensive computational modeling efforts have shown that GB-defect interactions including defect formation energy, defect mobility, defect boundary loading and absorption, local boundary structural transformations, and other defect-GB parameters can be heterogeneous as a function of the atomic GB structure.[19–23] To fully evaluate the GB-defect interactions under irradiation, careful consideration of the five macroscopic GB degrees of freedom to describe the misorientation and plane inclination is required. Further consideration is needed to account for possible non-equilibrium GB structures associated with severe plastic deformation[24] and far-from-equilibrium conditions.[25,26] GB-defect interactions also require assessment of the material system, irradiation type, energy, and temperature, and point defect product bias that can modify the mobility, concentration, and kinetics of defect migration near GBs. The myriad of important parameters detailed above provides a challenge to understanding the long-term radiation tolerance of individual GBs.

The concept of sink efficiency[27,28] provides a means to describe the affinity of the GB to absorb point defects from the adjacent matrix. The GB sink efficiency for point defects, such as vacancies, n_v, has previously been defined as:

$$n_v = \frac{J_v}{J_v^p} \tag{1}$$

where J_v is the actual vacancy flux to the GB and J_v^p is the vacancy flux to a perfect interface (e.g., a free surface).[29] Currently, there are no direct experimental methods to determine sink efficiency of individual GBs due to an inability to track, temporally and spatially, the local evolution of point defects under irradiation. However, several studies, highlighted below, have explored indirect methods to evaluate GB sink efficiency in pure metallic systems. One such method evaluates indirect sink efficiency by examining the spatial size and distribution of point defect clusters such as cavities and dislocation loops near the GB. The formation and coalescence of these irradiation-induced defect clusters rely on local nucleation from a supersaturation of point defects. In this respect, local defect (cavities or dislocation loops) denuded zones can form in regions adjacent to sinks, such as GBs, where there is insufficient defect supersaturation. Beyerlein et al.[29] correlated void denuded zones (VDZs) to the GB sink efficiency for vacancies following Eq. 2:

$$\lambda_{VDZ}\sqrt{\frac{K_{sv}}{D_v}} = \ln n_v - \ln\left(1 - \Delta c_v \frac{k_{sv}}{k_0}\right) \tag{2}$$

where λ_{VDZ} is the VDZ width adjacent to GBs, k_{sv} is the vacancy sink rate coefficient, k_0 is the defect production ratio, K_{sv} is a defect-sink reaction rate coefficient, D_v is the vacancy diffusivity, and c_v is the vacancy concentration.[29]

Several studies, highlighted below, evaluate the heterogeneous defect evolution through examination of the variation in defect denuded zone width as a function of GB character. All of the studies in FCC metals observe that the coherent Σ3 twin boundary has no denuded zone, while there are conflicting observations in the denuded zone width trends between high- and low-angle GBs. Importantly, many of these experimental studies rely on determination of the GB character through scanning electron microscopy (SEM) and transmission electron microscopy (TEM) orientation mapping techniques.[30,31] These orientation imaging techniques typically do not provide the full macroscopic GB character as the out-of-plane angle to account for the GB plane inclination cannot be easily determined, except under a limited set of circumstances, such as the Σ3 twin boundaries. Therefore, there is limited exploration into the GB plane inclination because of the experimental challenges detailed above; hence, there should be an emphasis of future work in this field. Han et al.[32] explored VDZ as a function of misorientation and GB plane inclination (exclusively for the Σ3 twin boundary plane) under helium irradiation between 300°C and 450°C in coarse-grained Cu. Figure 1 shows the significant variation in VDZ width found within the GB plane inclination for the Σ3 twin boundary misorientation. No VDZ was observed adjacent to the Σ3 coherent twin (111) boundary plane normal, while the Σ3 incoherent twin (112) boundary plane normal contained a VDZ width of ≈ 25 nm. Han et al. also showed that general random high-angle GBs (> 15° misorientation) had a large spread in VDZ widths, between 37 nm and 70 nm, with a slightly positive correlation with increasing misorientation angle. Zinkle and Farrell[33] examined void swelling in neutron-irradiated Cu between 250°C and 350°C and observed large VDZs between 300 nm and 700 nm along random GBs and incoherent twin boundaries, but not at coherent twin boundaries. The large anisotropic denuded zone formation among twin boundary planes was also reported in a model Ni alloy system after heavy ion irradiations at 500°C to ≈ 3.4 dpa.[34] The study observed no VDZ along the Σ3 coherent twin boundary, while the Σ3 incoherent twin had VDZ widths similar to random

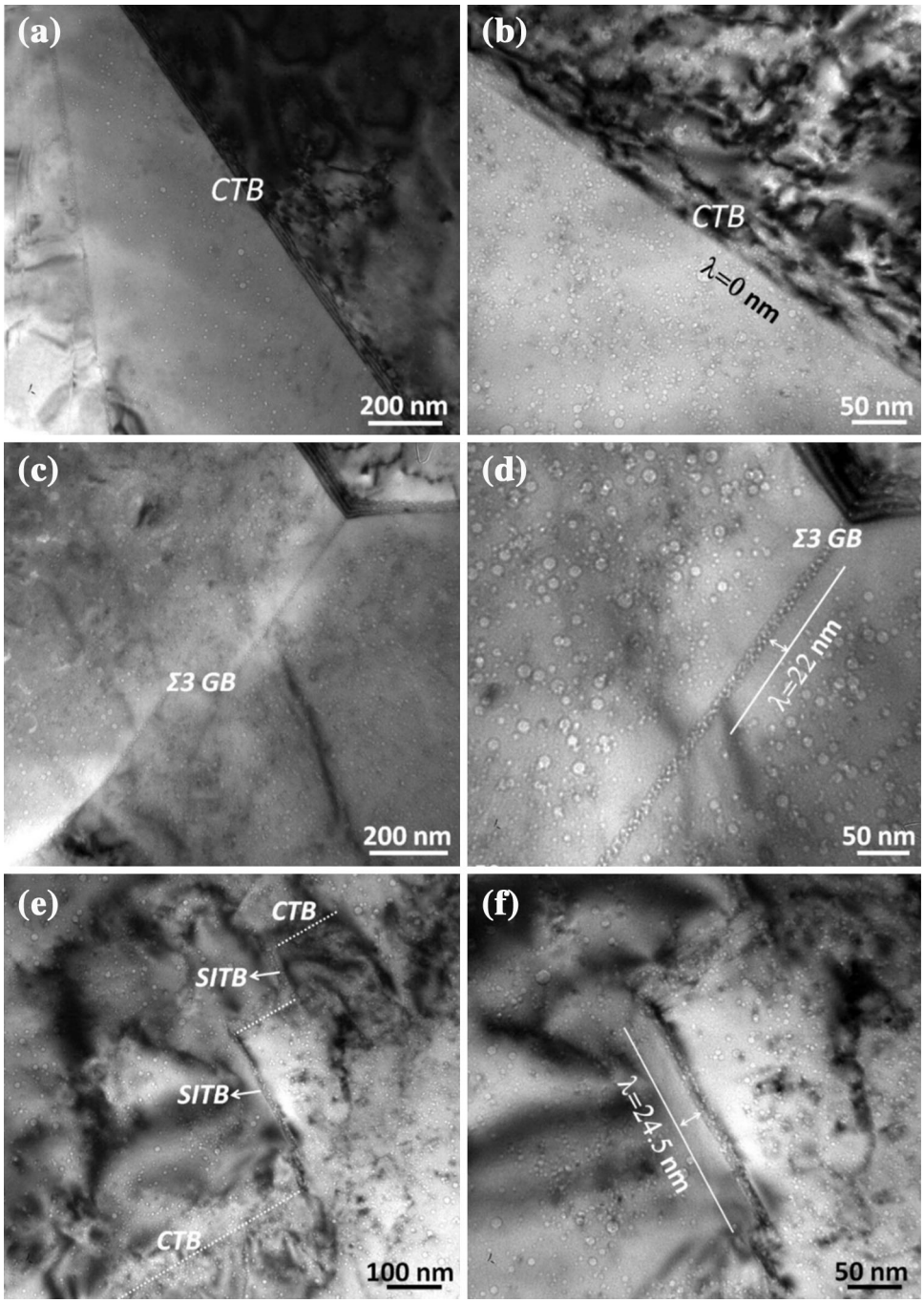

Fig. 1. Illustrations of variation in void denuded zones for the Σ3 <110> tilt grain boundaries in Cu irradiated at 450°C by 200 keV He ions with a fluence of 2×10^{17} ions cm^{-2}: (a, b) show radiation-induced voids but no void denuded zone near a coherent twin boundary; (c, d) show a void denuded zone near an asymmetric Σ3 <110> tilt grain boundary; (e, f) show a void denuded zone at the incoherent twin grain boundary. Image was reprinted from Han et al.[32], with permission from Elsevier.

high-angle GBs. Low-angle GBs (< 15° misorientations) were examined and had VDZ widths of the same magnitude as random high-angle GBs. The ability of low-angle GBs to accommodate point defects and subsequently form wide VDZs is consistent with work in polygonized high-purity Al where low-angle dislocation cell walls were observed to form VDZs after neutron irradiation.[35] Siegel et al.[36] examined stacking fault tetrahedra (SFT) denuded zones after elevated temperature non-equilibrium quenching in high-purity Au. High-temperature non-equilibrium quenching, although not an irradiation effect, provides a useful comparison because quenching can create a supersaturation of vacancies and subsequently SFTs. It was observed that both low-angle and non-special high-angle GBs operate as efficient sinks, whereas the Σ3 coherent twin boundary had significantly lower sink

efficiency. In contrast, Dollar and Gleiter[37] reported that both low-angle GBs and high-angle, low-energy GBs in coarse-grained high-purity Au have lower sink efficiency compared with random high-angle, high-energy GBs after room temperature irradiation with 150 keV Ar and post-irradiation annealing. The irradiation conditions in this study were different from the previous ones and the denuded zone width was evaluated at room temperature, and after post-irradiation annealing.

In nanocrystalline Fe with equiaxed grains irradiated with 10 keV He, El-Atwani et al.[38,39] observed He denuded zones at 427°C (but not at 300°C) where He-vacancy migration is expected. The effect of GB character on sink efficiency was explored by inspecting denuded zone formation for GBs of different misorientation angles, as shown in Fig. 2. It was found that both low- and high-angle GBs can be denuded or non-denuded, and no trend was observed for denuded zone formation as a function of misorientation angle. These results suggest that other parameters control the GB sink efficiency including the GB plane.[32]

The experimental literature continues to show conflicting observations regarding whether the GB atomic structure is a key factor in GB sink efficiency. While there is no ambiguity concerning the Σ3 coherent twins behaving as poor defect sinks under irradiation,[40] discrepancies exist on whether low-angle, special high-angle, and random high-angle GBs have discernable differences in sink efficiency. Computational modeling has aided in understanding GB-defect interactions related to sink efficiency. For example, Uberuaga et al.[41] showed that GB sink efficiency is non-static and evolves dynamically depending on how defects are accommodated in the GB, which is a function of the local GB atomic structure. Tschopp et al.[19] observed that both low- and high-angle GBs could be effective defect sinks for both vacancy and interstitial point defects through examination of the point defect formation energies. Atomistic and mesoscale modeling has been utilized to explore the effect of other factors on sink efficiency and GB atomic structure-defect interactions, but these computational predictions are beyond the scope of this perspective.[42–44] The reviewed experimental studies in pure and

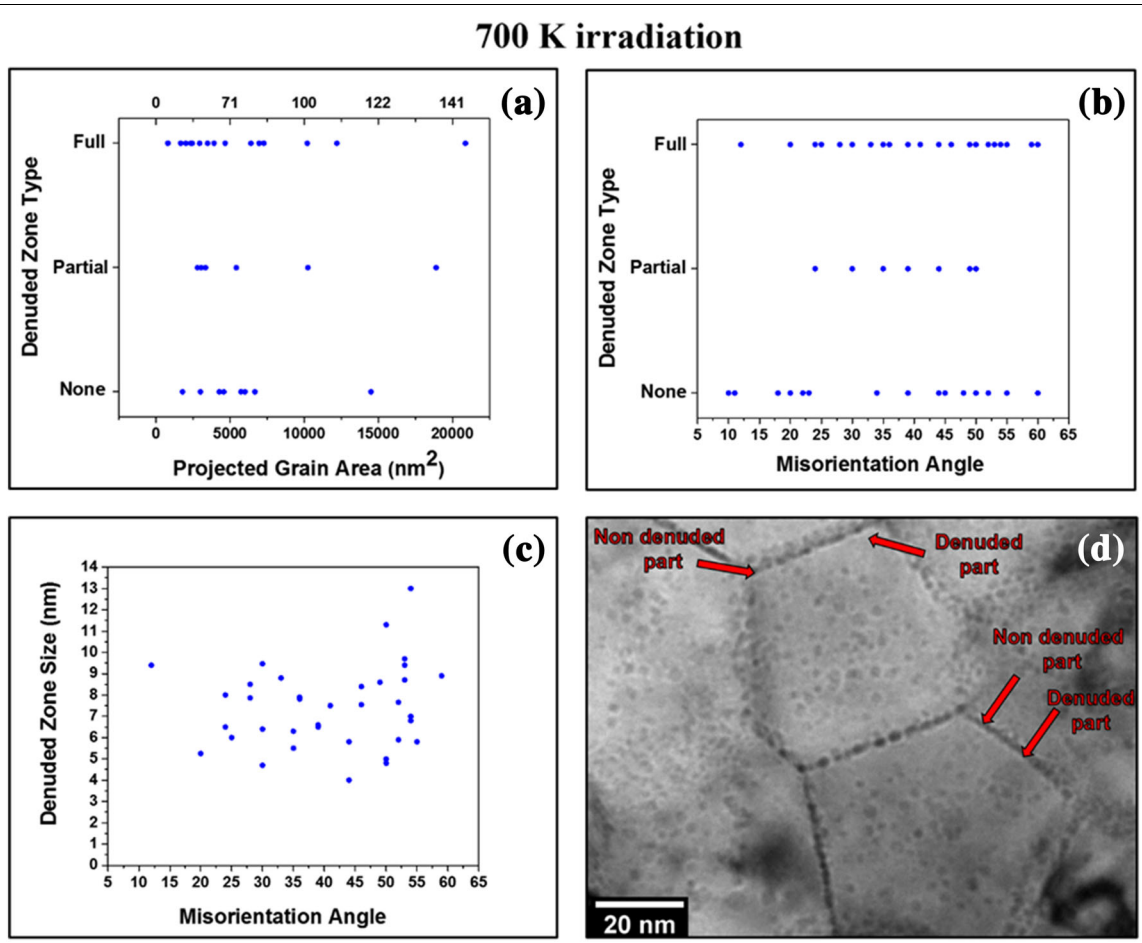

Fig. 2. Illustrations of variation in helium denuded zones in nanocrystalline Fe where (a, b) show the denuded zone type split into three categories: full denuded zone, partial denuded zone, and no denuded zone as a function of projected grain area (a), grain boundary misorientation angle (b); denuded zone width as a function of misorientation angle is shown in (c); (d) highlights a TEM micrograph with the three classifications of denuded zones. Image was reproduced from El-Atwani et al[38].

model systems suggest that the boundary misorientation and GB energy are insufficient parameters to correlate local GB sink efficiency trends under irradiation. Although experimentally challenging, improved methods relating the GB structure to sink efficiency are required which includes GB plane, microscopic GB degrees of freedom, and possible localized GB phase transitions under irradiation.

In addition, measuring the sink efficiency by denuded zone width may not be ideal. As emphasized by El-Atwani et al.,[45] using Eq. 2, even with no dislocation denuded zone formation, the sink efficiency can still be non-zero, which implies that GBs may still act as sinks with no apparent denuded zone formation. It was proposed that denuded zone formation can be related to the relative mobilities of vacancies and interstitials and that extra recombination of vacancies and interstitials at the GBs is a necessary requirement for denuded zone formation. The extent of the denuded zone depends on the disparity between defect mobilities. It was concluded that the relationship between sink efficiency and denuded zone width is not one to one. As a result, it is shown that the sink efficiency depends not only on the GB, but also on factors such as defect recombination rates in the grain interior.

An additional complication is the potential for heterogeneous defect sizes and density distributions in the vicinity of GBs under irradiation.[18,46–49] Under neutron irradiation as well as heavy ion and proton irradiations, the region adjacent to the VDZ has been reported to have enhanced void size, void density, and associated enhanced local swelling. The relative width and distribution of the non-uniform cavity distribution is a function of energetic irradiation species, temperature, and dose.[46,50] The heterogeneity of the cavity distribution adjacent to the denuded zone has been linked to defect production bias along with higher mobility and transport of glissile self-interstitial clusters to adjacent GBs.[46,51,52]

In addition to exploring the individual correlations between defect denuded zones and sink efficiency, nanocrystalline metals provide the opportunity to examine the role of a high GB density associated with a grain size reduction. The examination of grain size effects on irradiation has been an active research field over the past several decades and has been reviewed previously.[53,54] The interest in nanocrystalline materials is primarily related to the increase in GB density and corresponding defect sink density compared with their coarse-grained counterparts. Increased GB density in nanocrystalline and ultrafine-grained metals has been widely linked to an increase in Ni,[54] Fe,[26,38,39,55–57] Au,[58] Cu,[59,60] Pd,[61] Mo,[62] Pt,[63] and W.[56,64–66] Radiation tolerance is often defined in these studies as a reduction in defect (voids, helium bubbles, dislocation loops, or SFTs) density, size, or both. The common thread in all of the studies highlighted above is either the reduction in defect size and/or density with a grain size reduction. This trend does point towards the effectiveness of nanocrystalline materials in reducing the overall concentration of irradiation-induced defects within the grain interior compared with coarse-grained counterparts. However, the all-encompassing statement that radiation tolerance improves with a reduction in grain size must be carefully assessed, as some reports have shown that defect density does not always improve with a grain size reduction.[39,63,67] In these studies, factors such as the irradiation temperature, irradiation species, and irradiation-induced defect nature are highlighted as possible reasons for a lack of defect density trend with a grain size reduction into the nanocrystalline regime. For example, the lack of defect density reduction with grain size was observed in nanocrystalline Pt irradiated at 350°C with 2.8 MeV Au^{3+} ions to approximately 3 dpa.[63] In this case, no quantifiable difference in defect density was observed between 20 nm and 100 nm grains. The wide defect density scatter was attributed to stable sessile SFT defects adjacent to grain boundaries, which was reported in grain sizes down to 20 nm.

Defect Quantification Protocols

The varying literature on the radiation response, especially with some of the nanocrystalline and ultrafine-grained conditions highlighted above, is likely due, in part, to the difficult nature of quantifying dislocation loops, SFTs, and bubbles within small grains. Challenges result from two key aspects: (1) experimental difficulty of obtaining the correct imaging conditions for accurate defect identification and (2) defect counting issues and ambiguity. For the latter, traditional TEM-based defect imaging techniques[68] utilizing weak beam dark-field and kinematic two-beam bright-field imaging have been well established as a method to count dislocation loops, SFTs, cavities, and black-spot defects. However, due to the small nature of the nanocrystalline grains, especially with grains < 50 nm, the traditional protocols of tilting to multiple precise imaging conditions can become experimentally challenging and non-trivial. Recently, characterization techniques such as on-zone scanning TEM (STEM)-BF, STEM-annular BF, and STEM-annular DF[69] for dislocation imaging have been adapted for counting irradiation-induced dislocation loops and determining loop nature in coarse-grained Fe-based alloys. These adapted techniques could provide improved routes for quantifying radiation defects in nanocrystalline materials. The on-zone STEM imaging technique, detailed elsewhere,[69–71] provides the ability to utilize an imaging condition with reduced elastic contrast. In this approach, accurate defect counting requires only tilting or identifying grains on a single

on-zone condition. The difficulty of determining the exact and repeatable imaging condition under irradiation, especially with ultrafine and nanocrystalline-grained conditions, is likely a main cause for the reported large spread in experimental variations in defect size and density trends. Consistent imaging conditions and methodologies should be adopted to provide enhanced confidence in the reported defect size and density trends. In addition to the challenge of consistent imaging condition for quantifying defects, defect counting issues can arise from a lack of repeatability, human bias, and manual identification error.[72] Automated protocols for defect counting that utilize machine-learning and computer vision-based approaches[72–74] could provide an ideal avenue for defect analysis. Efforts to extend round-robin type defect imaging technique comparisons should be of benefit to the community at large. It is also apparent that sample preparation can be a large factor in reported defect statistics. This is particularly important for focused ion beam-based TEM sample preparation where defects can be introduced by the low-energy Ga beam during the thinning process to electron transparent thicknesses. It is therefore important to consider traditional methods such as electropolishing or methods to remove low-energy Ga-induced damage such as low-energy Ar polishing[75] or flash electropolishing.

Grain Boundary Migration Under Irradiation

In addition to the complex role of the local GB character and adjacent defect evolution under irradiation, the GB itself can become mobile during displacement damage events. This creates a moving target for the radiation damage to interact with. Although commonly treated as static in most radiation-related studies, GB migration due to other driving forces is well studied and an active field of materials research.[76–81]

Already in the 1980s, ion irradiation was observed to cause grain growth in thin films at temperatures where thermal effects alone did not induce any grain growth. The uniformity of grain growth combined with the irradiation dose dependence of grain size was found to be similar to the grain-growth behavior observed in isothermal annealing experiments (power law), which suggested that the driving forces are the same in both cases. Attempts to model grain growth by the thermal grain-growth models under irradiation were made,[82–84] all of which assumed the same driving force, the reduction of the total system free energy as a result of the global reduction in GB area.

In ion-irradiated Ni thin films, Wang et al.[85,86] found a linear trend of grain growth as a function of dose and a linear dependence of the grain-boundary mobility on the deposited damage energy. In 1988, Atwater and co-workers worked with Au, Ge, and Si thin films in a study of ion-induced grain growth[83] and found a dose dependence of grain size (D) varying from $D^4 \propto \Phi$ to $D^{1.96} \propto \Phi$ (where Φ is the dose). *Normal grain growth* was observed in all their irradiated thin films, even those that exhibited *abnormal grain growth* under purely thermal annealing conditions. Atwater reported a "weak" dependence of ion irradiation-induced grain growth on temperature. In the study, an atomistic model was proposed to describe the observed results of ion bombardment-enhanced grain growth. The model was based on independent processes all consisting of (1) the formation of a vacant site into which an atom can jump and (2) an atomic jump across the boundary into the vacant site. The model, which was ballistic in nature, did not take into account the intrinsic properties of the target materials (e.g., cohesive energy). It resulted in the prediction of a linear dependence of GB mobility on the defect generation rate and therefore failed to accurately describe the experimental results. Done around the same time, another study of ion-induced grain growth carried out by Liu and co-workers led to a very different model. In 1987–1990, Liu et al.[84,87] worked on pure metal thin films of Co, Ni, Cu, Pd, Pt, and Au and co-evaporated alloy systems of Ni-Co, Ni-Cu, and Pd-Pt. Liu's experimental results followed a power law in a similar way to Atwater's with an exponent averaging 3. The observation of significant variations in grain growth rates among systems that exhibit similar collisional damage behavior (namely Pt and Au as well as Ni-Cu alloys of different atomic concentrations) showed that a purely collisional model was inadequate to describe ion-induced grain growth and that intrinsic material properties (e.g., thermal conductivity and cohesive energy) must be taken into account in any attempt to model ion-induced GB mobility and thus ion-induced grain growth under irradiation. Furthermore, it was observed that greater grain growth was induced in those materials with low cohesive energy, ΔH_{coh}. By assuming the activation energy for grain growth scales with the cohesive energy, GB mobility was related to the cohesive energy of the material. Finally, Liu suggested that ion irradiation-induced grain growth, and thus the GB mobility could be related to the "thermal spike" effects of ion irradiation. Indeed, it was implied that the mobility of GBs depends on the number of atomic jumps generated in a thermal spike expressed in Vineyard's analysis of thermal spikes.[88,89] For thermal spikes of cylindrical geometry, it was proposed that the mobility of GBs varied with $\frac{F_D^2}{\Delta H_{coh}^2}$. In 1989–1992, Alexander and co-workers further supported the application of the thermal spike model to ion-induced grain growth with their studies of the ion-irradiated binary systems.[82,90,91] In all the films, normal grain growth was induced by

irradiation with the average grain size increasing with ion dose according to:

$$\overline{D}^n - \overline{D}_0^n = K\Phi \quad (3)$$

where D is the average grain size, Φ is the dose, and K is related to the mobility of the GB under irradiation. Despite observed grain growth exponents spanning values from 1.9 to 4.3 (averaging $n = 3$), Alexander et al. associated deviations from ideal parabolic ($n = 2$) grain growth kinetics with the drag effect of inhibiting driving forces. Their observations supported the idea that a purely collisional model could not accurately describe ion-induced grain growth and that properties of the material should be taken into account, implying that GB mobility under irradiation will depend on both material properties and irradiation parameters. The thermal spike model of ion irradiation grain growth developed by Alexander incorporated grain curvature and chemical gradients as the driving forces for atomic migration across boundaries within thermal spikes and found a grain-boundary mobility of (with F_D being the damage energy deposition density), in contrast with that proposed by Liu, $\frac{F_D^2}{\Delta H_{coh}^2}$. The model successfully accounted for ion irradiation-induced grain growth in co-evaporated alloy films where the sole driving force considered was boundary curvature, but it failed to describe observed grain growth data in multilayer thin films. Noticeably, Alexander's model ignored the irradiation-induced defect cascade structure (with subcascade formation), an important feature of ion irradiation that is expected to vary considerably among different ion target combinations and lead to varying grain growth behavior.[92] This important feature of ion irradiation-induced damage was finally incorporated in the model developed by Kaoumi et al.[93] to describe the kinetics of grain growth under irradiation, giving the thermal spike-based model a realistic basis. The study employed in situ ion irradiation TEM observations in Pt, Au, Cu, and Zr and found significant GB migration as a result of displacement damage, as illustrated in Fig. 3.[93] Through detailed grain size measurements taken from individual still frames captured during the in situ study, a statistical representation of the grain size distribution as a function of nanocrystalline metal bombarded, ion species, and ion flux was obtained and used to develop the analytical model. Other systematic in situ ion irradiation TEM experiments have studied the grain growth evolution of nanocrystalline metallic Cu-Fe and Zr-Fe thin films, which highlighted a dragging effect on the kinetics of grain growth under irradiation.[94–96] A theoretical model of grain growth under ion irradiation was developed (for low temperatures where thermal grain-boundary migration is not observed, i.e., $0.2T_{melting}$), based on the direct impact of irradiation-induced thermal spikes on GBs. The model described grain growth (in pure metals) as being driven solely by the reduction of GB area. GB migration occurs by atomic jumps within the thermal spike biased by the GB curvature driving force.[93] In contrast with previous models of grain growth under ion irradiation, which ignored the nature of the cascade structure, this model incorporated cascade structure features such as subcascade formation and the probability of subcascades occurring at grain boundaries. The model yielded a power law expression relating the average grain size with the ion dose, with an exponent of $n = 3$, which was in good agreement with the experimental data and was found to be an inherent feature of grain growth under ion irradiation; it related the mobility of the GB under irradiation with the collisional properties of the material as well as the intrinsic material properties.

More recently, a similar in situ ion irradiation TEM experiment on nanocrystalline Au was performed with the addition of crystallographic orientation and GB character information through the incorporation of automated crystal orientation mapping (ACOM).[97] This addition not only provided a computational tool to rapidly characterize the grain size distribution as a function of dose, but it also provided insight into the local GB migration as a function of GB misorientation, as can be seen in Fig. 4. Figure 4 highlights the before and after correlation of a site-specific region of localized grain growth in nanocrystalline Au and associated grain growth. In one case, a GB (labeled as Grain "1") with a medium misorientation (15°–30°) appears to migrate until reaching a sequence of low-angle (subgrain) boundaries (< 3°), as shown in Fig. 4g, h, i, and j.[97] The ability to couple ACOM and related orientation mapping techniques provides a path forward to explore local GB structure and orientation texture effects on GB migration and irradiation-induced grain growth in general.

FUTURE DIRECTIONS

The future is bright for experimental investigations of the interplay between radiation damage and complex interfaces, including GBs, because of the recent development of integrated structural and chemical characterization tool sets as well as the rapid development in data analytics. Advancements in these areas provide not only the ability to interpret the contributions from second- and third-order factors influencing this complicated interplay, but also provide a stronger coupling to theory and modeling efforts.

The path toward comprehending the role of GB structure during irradiation is two-pronged: understanding both the role of the individual GB structures and GB network along with the potential role of GB migration. Further experimental methodologies to probe GB-defect evolution during irradiation could be developed to answer the following outstanding questions:

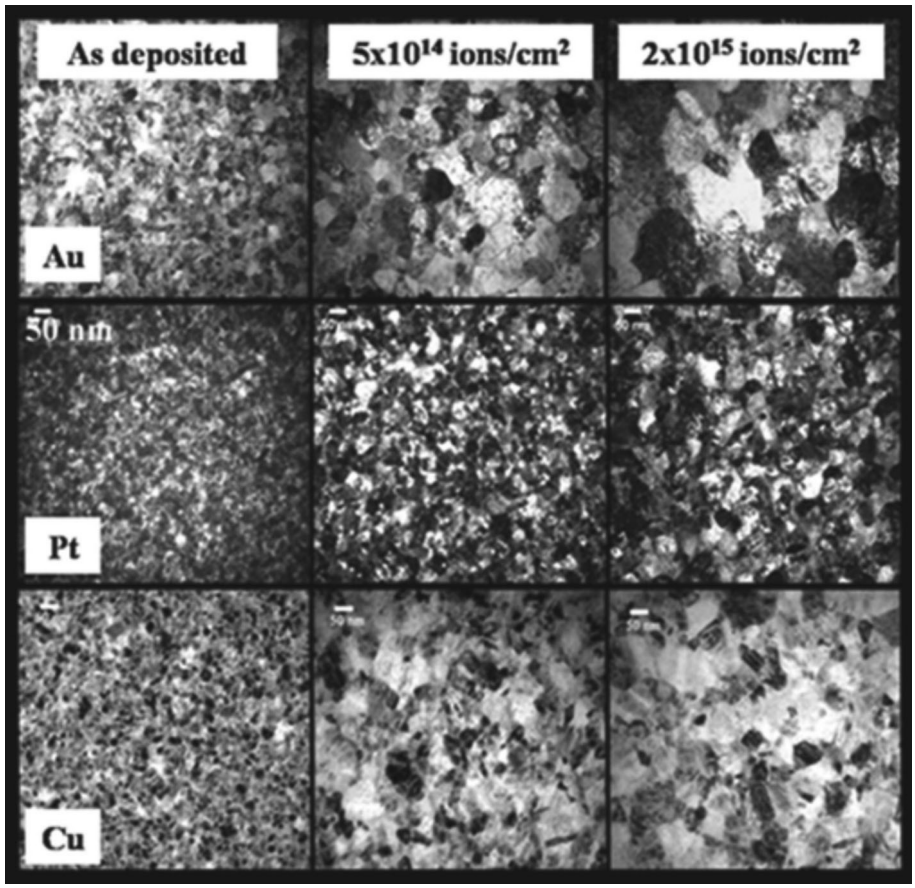

Fig. 3. Sequence of bright-field TEM micrographs taken at a range of ion doses showing grain growth induced by ion irradiation at room temperature; from left to right: as deposited, 5×10^{14} ions/cm^2, 2×10^{15} ions/cm^2; from top to bottom: Au irradiated with 500 keV Ar ions, Pt irradiated with 500 keV Ar ions, and Cu irradiated with 500 keV Kr ions. Image reprinted from Kaoumi et al.[93], with the permission of AIP Publishing.

- How does the local GB structure change as it accommodates irradiation-induced defects and defect clusters including potential formation of extrinsic boundary dislocations and boundary disconnections phase transitions?
- How does GB migration affect the local defect evolution? For example, how does boundary migration modify local defect denuded zones adjacent to the GB?

To understand the latter, a detailed understanding of the role defect structures play in GB motion is needed. There is emerging insight from the computation materials science community suggesting that the "roughness" of the GB at the atomic scale will greatly impact the mobility of some GBs.[4] This prediction has not yet been experimentally verified, but advancements in both aberration-corrected TEM and stable high-temperature in situ TEM heating stages may change that in the near future. Beyond individual grain boundary studies, the migration of GBs has been correlated to the surrounding GB network and specifically the drag of the triple points connecting GBs.[98] Advancements in accounting for the local GB network effects including triple junctions and twin boundary networks[99,100] should provide further insight into irradiation-induced grain growth. To examine the local GB structure accommodation of irradiation-induced defects, experimental efforts are needed to combine atomic resolution imaging of the local GB structure with sequential irradiation. In these studies, the evolution of the local atomic GB structure could be examined as a function of irradiation dose. Indeed, probing the irradiation-induced evolution of the internal GB structure may require the development of an aberration-corrected in situ ion irradiation S/TEM, a facility that has yet to be developed.

Although not the focus of this review, the impact of chemical additions to the radiation tolerance of GBs and interfaces will be significant. Radiation damage has long been known to induce both mixing and segregation of solutes in alloys,[101] but recent developments in chemical mapping with nanometer resolution via atom probe tomography and high-resolution STEM spectroscopy techniques have permitted new insight into the complex interactions.[14,102] In addition to RIS and ion beam mixing effects, solute modification can be used as a tool to alter the internal GB structure (GB phase and/or

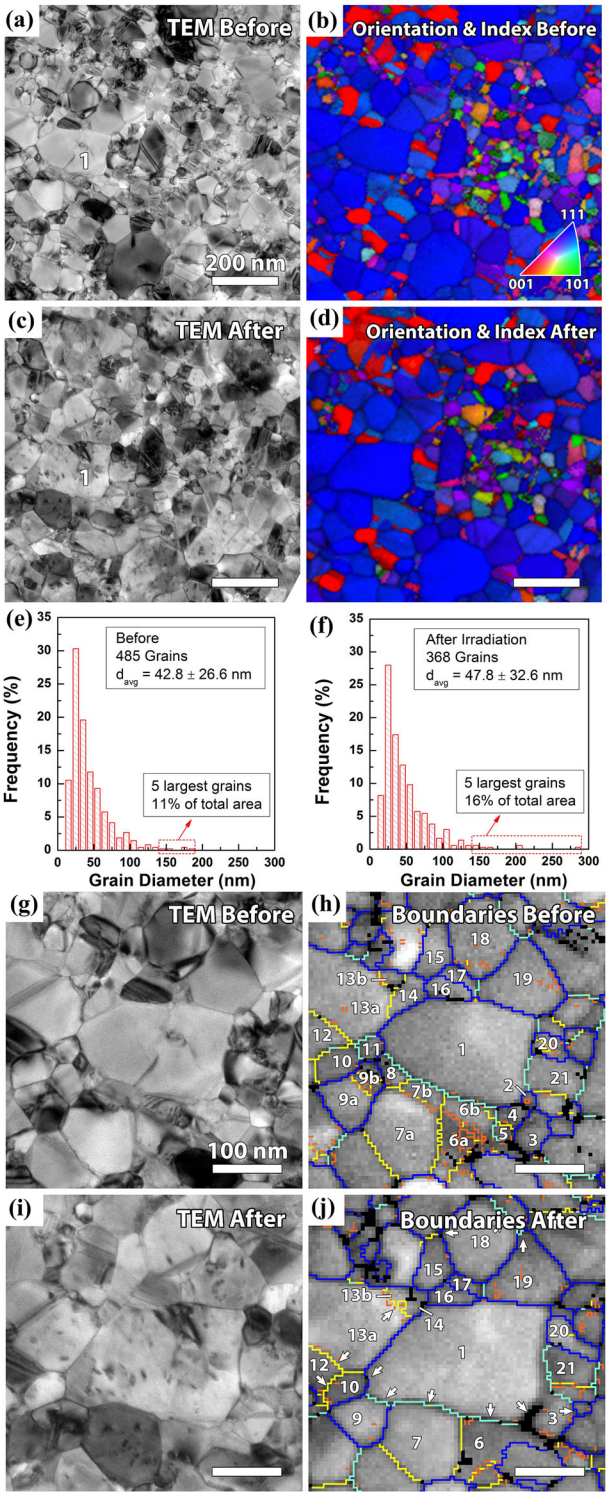

◀Fig. 4. Illustrations of both global and boundary specific grain growth during heavy ion irradiation from Bufford et al.[97] TEM images (a, c) and inverse pole figure colored orientation maps with index data overlaid (b, d) were collected from the same area before (a, b) and after (c, d) irradiation with a dose of 2×10^{15} cm^{-2} with 10 MeV Si^{3+}. Grain size was determined and is shown in the histograms from before (e) and after (f) irradiation conditions. Local boundary migration is shown in images (g–j) where grain 1 is shown to migrate downwards into a series of preexisting grains (labeled). Orange, yellow, cyan, and blue indicate grain boundaries with misorientation angles in the respective ranges of 0°–3°, 3°–15°, 15°–30°, and ≥ 30°. Images are reprinted from Bufford et al.[97], with the permission of AIP Publishing (Color figure online).

stability the GB network).[103–105] One such approach is given by Schuler et al.[105] where trends in the enthalpy of mixing, enthalpy of segregation, and atomic size mismatch between the solute–solvent are highlighted in Fig. 5 for a series of binary alloys. The selection rules for amorphous intergranular film (GB complexion) formation include a positive enthalpy of segregation and negative enthalpy of mixing. Amorphous intergranular GB phases have been shown through computation modeling to enhance GB sink efficiency under irradiation.[106] This demonstrates the need to investigate the role of chemistry on the interaction between radiation damage and the underlying GB structure including GB solute ordering and disordering.

Finally, one of the greatest advancements expected to impact our understanding of radiation defect interplay with GBs will be the incorporation of advanced data analytics. If properly integrated, this will permit the elimination of the often flawed and extremely time-consuming manual analysis of radiation damage. Recent studies have made great progress[72–74] in this area and provide a roadmap to increase the speed and reliability of defect counting. The digitization of defect counting increases the information gained on the spatial and temporal evolution of the radiation damage and provides the potential for overlaying the data onto the structural and chemical maps of the evolving sample, provided by, for example, ACOM and energy-dispersive x-ray spectroscopy. The ability to process complex spectral analysis will require a strongly collaborative effort combining the expertise of diffraction physicists, metallurgists, radiation physicists, and advanced data scientists. Linking advanced structural and chemical characterization capabilities with the ability to process and incorporate large data sets into predictive models provides the opportunity to more fully elucidate the interaction of radiation defects with the underlying and evolving microstructure.

CONCLUSION

Most classical theories and current models treat GBs as stable and constant features to absorb radiation defects. In contrast, many recent experiments highlighted in this brief review have shown a wide range of interplay mechanisms between GBs and irradiation-induced defects in both time and space. These experimental results are often conflicting, resulting in significant confusion in the community. GB sink efficiency and associated defect denuded zones are heterogeneous as a function of the GB character. However, there is no consensus

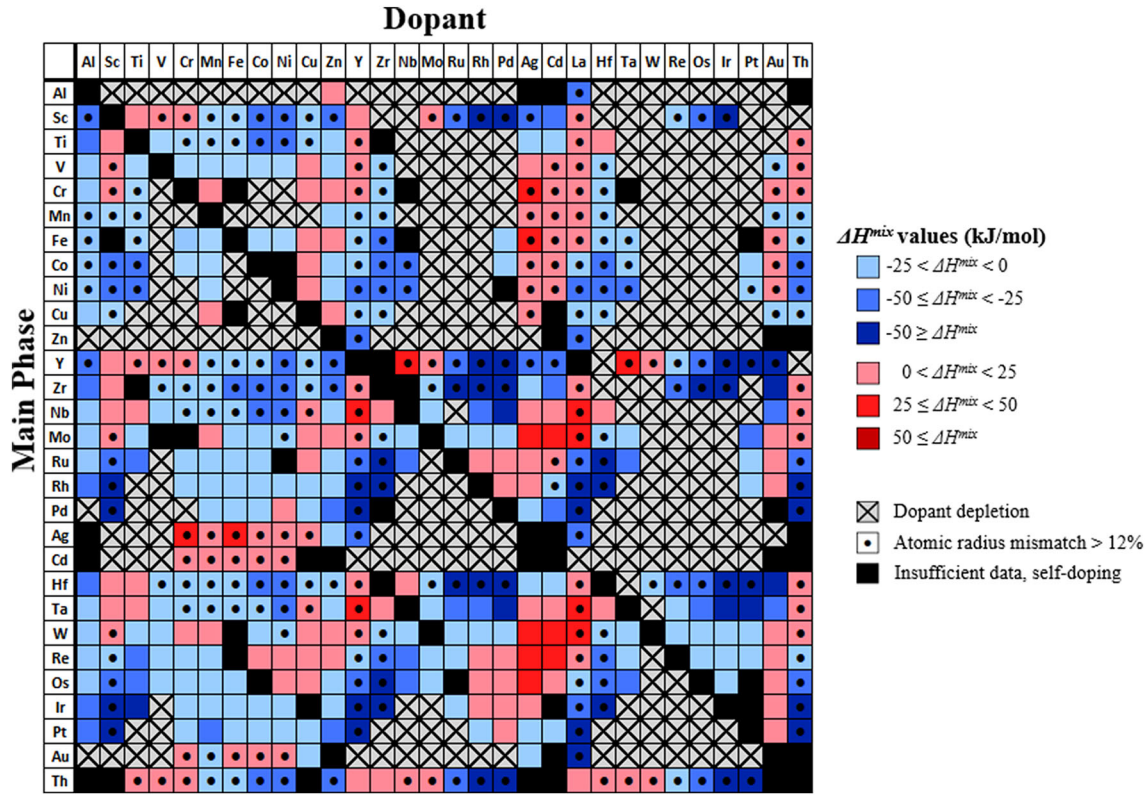

Fig. 5. A schematic of various solvent and solute (dopants) pairs for binary alloys where the box color shows the level of enthalpy of mixing between solvent–solute; systems with a positive enthalpy of segregation and negative enthalpy of mixing (blue boxes) as detailed by Schuler and Rupert[105] are a key selection criterion for the formation of amorphous intergranular films. Image reproduced from Schuler et al.[105] with permission from Elsevier (Color figure online).

on the key aspects of the experimentally determined GB character that result in a variation in the sink efficiency. To further complicate the dynamics between GBs and radiation damage, experiments have shown that GB migration can occur because of displacement damage and is dependent on the GB character, local radiation environment, and probably the interconnected nature of the microstructure. The combination of radiation-induced GB migration and evolving defect sink efficiency makes the response of GBs difficult to predict. Advanced experimental efforts coupled with refined computational models are needed to fully understand the governing mechanisms and influencing factors associated with the complex GB-radiation defect interaction and temporal evolution.

ACKNOWLEDGEMENTS

The authors thank Drs. Claire Chisholm and Brad Boyce for useful discussions. The time of C.M.B. and K.H. was fully supported by the US Department of Energy, Office of Basic Energy Sciences, Division of Materials Sciences and Engineering. This work was performed, in part, at the Center for Integrated Nanotechnologies, an Office of Science User Facility operated for the US Department of Energy (DOE) Office of Science. Sandia National Laboratories is a multi-mission laboratory managed and operated by National Technology and Engineering Solutions of Sandia, LLC, a wholly owned subsidiary of Honeywell International, Inc., for the US DOE's National Nuclear Security Administration under contract DE-NA-0003525. Los Alamos National Laboratory, an affirmative action, equal opportunity employer, is operated by Los Alamos National Security, LLC, for the National Nuclear Security Administration of the US DOE under contract DE-AC52-06NA25396. The views expressed in the article do not necessarily represent the views of the US DOE or the United States Government.

REFERENCES

1. S.J. Zinkle and G.S. Was, *Acta Mater.* 61, 735 (2013).
2. D.L. Olmsted, S.M. Foiles, and E.A. Holm, *Acta Mater.* 57, 3694 (2009).
3. F. Abdeljawad, S.M. Foiles, A.P. Moore, A.R. Hinkle, C.M. Barr, N.M. Heckman, K. Hattar, and B.L. Boyce, *Acta Mater.* 158, 440 (2018).
4. D.L. Olmsted, S.M. Foiles, and E.A. Holm, *Scr. Mater.* 57, 1161 (2007).
5. J.L. Priedeman, C.W. Rosenbrock, O.K. Johnson, and E.R. Homer, *Acta Mater.* 161, 431 (2018).
6. E.R. Homer, S. Patala, and J.L. Priedeman, *Sci. Rep.* 5, 15476 (2015).
7. G.S. Rohrer, *J. Mater. Sci.* 46, 5881 (2011).
8. G. Odette, M. Alinger, and B. Wirth, *Annu. Rev. Mater. Res.* 38, 471 (2008).
9. A. Misra and L. Thilly, *MRS Bull.* 35, 965 (2010).

10. X. Zhang, K. Hattar, Y. Chen, L. Shao, J. Li, C. Sun, K. Yu, N. Li, M.L. Taheri, and H. Wang, *Prog. Mater. Sci.* 96, 217 (2018).
11. R. Andrievski, *J. Mater. Sci.* 38, 1367 (2003).
12. G.R. Odette, *JOM* 66, 2427 (2014).
13. I. Beyerlein, A. Caro, M. Demkowicz, N. Mara, A. Misra, and B. Uberuaga, *Mater. Today* 16, 443 (2013).
14. A.J. Ardell and P. Bellon, *Curr. Opin. Solid State Mater. Sci.* 20, 115 (2016).
15. G.S. Was, *Fundamentals of Radiation Materials Science: Metals and Alloys*, 1st ed. (Berlin: Springer, 2007).
16. B.N. Singh, *Nat. Phys. Sci.* 244, 142 (1973).
17. B.N. Singh and A.J.E. Foreman, *Philos. Mag.* 29, 847 (1974).
18. B.N. Singh, M. Eldrup, S.J. Zinkle, and S.I. Golubov, *Philos. Mag. A* 82, 1137 (2002).
19. M.A. Tschopp, K.N. Solanki, F. Gao, X. Sun, M.A. Khaleel, and M.F. Horstemeyer, *Phys. Rev. B* 85, 064108 (2012).
20. X.-M. Bai, A.F. Voter, R.G. Hoagland, M. Nastasi, and B.P. Uberuaga, *Science* 327, 1631 (2010).
21. A. Dunn, R. Dingreville, E. Martínez, and L. Capolungo, *Acta Mater.* 110, 306 (2016).
22. X.-M. Bai, L.J. Vernon, R.G. Hoagland, A.F. Voter, M. Nastasi, and B.P. Uberuaga, *Phys. Rev. B* 85, 214103 (2012).
23. T. Frolov, D.L. Olmsted, M. Asta, and Y. Mishin, *Nat. Commun.* 4, 1899 (2013).
24. X. Sauvage, G. Wilde, S.V. Divinski, Z. Horita, and R.Z. Valiev, *Mater. Sci. Eng. A* 540, 1 (2012).
25. G.J. Tucker and D.L. McDowell, *Int. J. Plast.* 27, 841 (2011).
26. G.A. Vetterick, J. Gruber, P.K. Suri, J.K. Baldwin, M.A. Kirk, P. Baldo, Y.Q. Wang, A. Misra, G.J. Tucker, and M.L. Taheri, *Sci. Rep.* 7, 12275 (2017).
27. R.W. Balluffi, *J. Nucl. Mater.* 69–70, 117 (1978).
28. A.P. Sutton and R.W. Balluffi, *Interfaces in Crystalline Materials*, Oxford Classic Series 2006 (Oxford University Press, New York, NY, 1995).
29. I. Beyerlein, M. Demkowicz, A. Misra, and B. Uberuaga, *Prog. Mater. Sci.* 74, 125 (2015).
30. E.F. Rauch and M. Véron, *Mater. Charact.* 98, 1 (2014).
31. P.W. Trimby, *Ultramicroscopy* 120, 16 (2012).
32. W. Han, M. Demkowicz, E. Fu, Y. Wang, and A. Misra, *Acta Mater.* 60, 6341 (2012).
33. S.J. Zinkle and K. Farrell, *J. Nucl. Mater.* 168, 262 (1989).
34. C.M. Barr, L. Barnard, J.E. Nathaniel, K. Hattar, K.A. Unocic, I. Szlurfarska, D. Morgan, and M.L. Taheri, *J. Mater. Res.* 30, 1290 (2015).
35. A. Horsewell and B.N. Singh, "Role of dislocations, dislocation walls, and grain boundaries in void formation during early stages of fast neutron irradiation." *Effects of Radiation on Materials: 12th International Symposium*, STP870, ed. F.A. Garner and J.S. Perrin (Williamsburg, VA: ASTM, 1985).
36. R.W. Siegel, S.M. Chang, and R.W. Balluffi, *Acta Metall.* 28, 249 (1980).
37. M. Dollar and H. Gleiter, *Scr. Metall.* 19, 481 (1985).
38. O. El-Atwani, J. Nathaniel II, A. Leff, J. Baldwin, K. Hattar, and M. Taheri, *Mater. Res. Lett.* 5 (3), 195 (2016).
39. O. El-Atwani, J. Nathaniel, A. Leff, B. Muntifering, J. Baldwin, K. Hattar, and M. Taheri, *J. Nucl. Mater.* 484, 216 (2017).
40. M.J. Demkowicz, O. Anderoglu, X. Zhang, and A. Misra, *J. Mater. Res.* 26, 1666 (2011).
41. B.P. Uberuaga, L.J. Vernon, E. Martinez, and A.F. Voter, *Sci. Rep.* 5, 7801 (2015).
42. Y. Zhang, H. Huang, P.C. Millett, M. Tonks, D. Wolf, and S.R. Phillpot, *J. Nucl. Mater.* 422, 69 (2012).
43. C. Jiang, N. Swaminathan, J. Deng, D. Morgan, and I. Szlufarska, *Mater. Res. Lett.* 2, 100 (2013).
44. H. Jiang and I. Szlufarska, *Sci. Rep.* 8, 147 (2018).
45. O. El-Atwani, E. Martinez, E. Esquivel, M. Efe, C. Taylor, Y.Q. Wang, B.P. Uberuaga, S.A. Maloy, *Phys. Rev. Mater.* 2, 113604 (2018). https://doi.org/10.1103/PhysRevMaterials.2.113604.
46. H. Trinkaus, B.N. Singh, and M. Victoria, *J. Nucl. Mater.* 233, 1089 (1996).
47. A.J.E. Foreman, B.N. Singh, and A. Horsewell, *Mater. Sci. Forum* 15–18, 895 (1987).
48. B.N. Singh and T. Leffers, *J. Nucl. Mater.* 105, 1 (1982).
49. J.O. Stiegler and E.E. Bloom, *Radiat. Effects* 8, 33 (1971).
50. B.N. Singh and S.J. Zinkle, *J. Nucl. Mater.* 217, 161 (1994).
51. H. Trinkaus, B.N. Singh, and A.J.E. Foreman, *J. Nucl. Mater.* 199, 173 (1992).
52. H. Trinkaus, B.N. Singh, and A.J.E. Foreman, *J. Nucl. Mater.* 206, 212 (1993).
53. X. Zhang, K. Hattar, Y. Chen, L. Shao, J. Li, C. Sun, K. Yu, N. Li, M.L. Taheri, H. Wang, J. Wang, and M. Nastasi, *Prog. Mater. Sci.* 96, 217 (2018).
54. C. Sun, M. Song, K.Y. Yu, Y. Chen, M. Kirk, M. Li, H. Wang, and X. Zhang, *Metall. Mater. Trans. A* 44, 1966 (2013).
55. G. Vetterick, *Radiation Damage in Nanocrystalline Iron, Materials Science and Engineering* (Philadelphia: Drexel University, 2014).
56. O. El-Atwani, K. Hattar, J.A. Hinks, G. Greaves, S.S. Harilal, and A. Hassanein, *J. Nucl. Mater.* 458, 138 (2015).
57. K.Y. Yu, Y. Liu, C. Sun, H. Wang, L. Shao, E.G. Fu, and X. Zhang, *J. Nucl. Mater.* 425, 140 (2012).
58. Y. Chimi, A. Iwase, N. Ishikawa, M. Kobiyama, T. Inami, and S. Okuda, *J. Nucl. Mater.* 297, 355 (2001).
59. Y. Chen, J. Li, K.Y. Yu, H. Wang, M.A. Kirk, M. Li, and X. Zhang, *Acta Mater.* 111, 148 (2016).
60. J. Li, K.Y. Yu, Y. Chen, M. Song, H. Wang, M.A. Kirk, M. Li, and X. Zhang, *Nano Lett.* 15, 2922 (2015).
61. M. Rose, A.G. Balogh, and H. Hahn, *Nucl. Instrum. Methods Phys. Res. B* 127, 119 (1997).
62. G.M. Cheng, W.Z. Xu, Y.Q. Wang, A. Misra, and Y.T. Zhu, *Scr. Mater.* 123, 90 (2016).
63. C.M. Barr, N. Li, B.L. Boyce, and K. Hattar, *Appl. Phys. Lett.* 112, 181903 (2018).
64. O. El-Atwani, J.A. Hinks, G. Greaves, S. Gonderman, T. Qiu, M. Efe, and J.P. Allain, *Sci. Rep.* 4, 4716 (2014).
65. O. El-Atwani, J. Hinks, G. Greaves, J.P. Allain, and S.A. Maloy, *Mater. Res. Lett.* 5, 343 (2017).
66. O. El-Atwani, E. Esquivel, E. Aydogan, E. Martinez, J.K. Baldwin, M. Li, B.P. Uberuaga, and S.A. Maloy, *Acta Mater.* 165, 128 (2019). https://doi.org/10.1016/j.actamat.2018.11.024.
67. O. El-Atwani, A. Suslova, T.J. Novakowski, K. Hattar, M. Efe, S.S. Harilal, and A. Hassanein, *Mater. Charact.* 99, 68 (2015).
68. M.L. Jenkins and M.A. Kirk, *Characterisation of Radiation Damage by Transmission Electron Microscopy* (Philadelphia: Institute of Physics Publishing, 2000).
69. C.M. Parish, K.G. Field, A.G. Certain, and J.P. Wharry, *J. Mater. Res.* 30, 1275 (2015).
70. B. Yao, D.J. Edwards, and R.J. Kurtz, *J. Nucl. Mater.* 434, 402 (2013).
71. P.J. Phillips, M.C. Brandes, M.J. Mills, and M. De Graef, *Ultramicroscopy* 111, 1483 (2011).
72. W. Li, K.G. Field, and D. Morgan, *NPJ Comput. Mater.* 4, 36 (2018).
73. H. Yu, X. Yi, and F. Hofmann, *Ultramicroscopy* 195, 653 (2018).
74. X. Yi, A.E. Sand, D.R. Mason, M.A. Kirk, S.G. Roberts, K. Nordlund, and S.L. Dudarev, *EPL (Europhys. Lett.)* 110, 36001 (2015).
75. A. Aitkaliyeva, J.W. Madden, B.D. Miller, and J.I. Cole, *Micron* 67, 65 (2014).
76. V.E. Fradkov and L.S. Shvindlerman, *Phys. Chem. Mech. Surf.* 9, 180 (1982).
77. G. Gottstein and L.S. Shvindlerman, *Grain Boundary Migration in Metals: Thermodynamics* (Kinetics: Applications, CRC Press, Boca Raton, 2009).
78. T. Rupert, D. Gianola, Y. Gan, and K. Hemker, *Science* 326, 1686 (2009).

79. D. Turnbull, *JOM* 3, 242 (1951).
80. C. Braun, J.M. Dake, C.E. Krill, and R. Birringer, *Sci. Rep.* 8, 1592 (2018).
81. J. Han, S.L. Thomas, and D.J. Srolovitz, *Prog. Mater. Sci.* 98, 386 (2018).
82. D.E. Alexander and G.S. Was, *Phys. Rev. B* 47, 14 (1993).
83. H.A. Atwater, C.V. Thompson, and H.I. Smith, *J. Appl. Phys.* 64, 2354 (1988).
84. J.C. Liu, M. Nastasi, and J.W. Mayer, *J. Appl. Phys.* 62, 423 (1987).
85. P. Wang, D.A. Thompson, and W.W. Smeltzer, *Nucl. Instrum. Methods Phys. Res. Sect. B Beam Interact. Mater. Atoms* 7–8, 97 (1985).
86. P. Wang, D.A. Thompson, and W.W. Smeltzer, *Nucl. Instrum. Methods Phys. Res. Sect. B Beam Interact. Mater. Atoms* 16, 17 (1986).
87. J.C. Liu, J. Li, and J.W. Mayer, *J. Appl. Phys.* 67, 2354 (1990).
88. G.J. Dienes and G.H. Vineyard, *Radiat. Effects Solids* 40, 1361 (1918).
89. G.H. Vineyard, *Radiat. Effects* 29, 245 (1976).
90. D.E. Alexander, G.S. Was, and L.E. Rehn, *Nucl. Instrum. Methods Phys. Res.* B59/60, 462 (1991).
91. D.E. Alexander, G.S. Was, and L.E. Rehn, *J. Appl. Phys.* 70, 1252 (1991).
92. D.E. Alexander and G.S. Was, *Surf. Coat. Technol.* 51, 8174 (1992).
93. D. Kaoumi, A.T. Motta, and R.C. Birtcher, *J. Appl. Phys.* 104, 073525 (2008).
94. D. Kaoumi, A. Motta, and R.C. Birtcher, *J. ASTM Int.* 4, 687 (2007).
95. D. Kaoumi, A.T. Motta, and R.C. Birtcher, *J. Nucl. Mater.* 382, 184 (2008).
96. D. Kaoumi, A.T. Motta, and R.C. Birtcher, *Nucl. Instrum. Methods Phys. Res. Sect. B (Beam Interact. Mater. Atoms)* 242, 490 (2006).
97. D. Bufford, F. Abdeljawad, S. Foiles, and K. Hattar, *Appl. Phys. Lett.* 107, 191901 (2015).
98. U. Czubayko, V. Sursaeva, G. Gottstein, and L. Shvindlerman, *Acta Mater.* 46, 4527 (1998).
99. B.W. Reed and M. Kumar, *Scr. Mater.* 54, 1029 (2006).
100. C.M. Barr, A.C. Leff, R.W. Demott, R.D. Doherty, and M.L. Taheri, *Acta Mater.* 144, 281 (2018).
101. R.S. Averback, *Nucl. Instrum. Methods Phys. Res. B* 15, 2458 (1986).
102. S. Chee, B. Stumphy, N. Vo, R. Averback, and P. Bellon, *Acta Mater.* 58, 4088 (2010).
103. T. Chookajorn, H.A. Murdoch, and C.A. Schuh, *Science* 337, 951 (2012).
104. S.J. Dillon, M. Tang, W.C. Carter, and M.P. Harmer, *Acta Mater.* 55, 6208 (2007).
105. J.D. Schuler and T.J. Rupert, *Acta Mater.* 140, 196 (2017).
106. J.E. Ludy and T.J. Rupert, *Scr. Mater.* 110, 37 (2016).